Carbon Capture Science & Technology 7 (2023) 100111

Contents lists available at ScienceDirect

Carbon Capture Science & Technology

journal homepage: www.elsevier.com/locate/ccst

Full Length Article

On the exergy efficiency of CO_2 capture: The relation between sub-process and overall efficiencies

David Berstad [a,*], Truls Gundersen [b]

[a] SINTEF Energy Research, Sem Sælands vei 11, Trondheim NO-7034, Norway
[b] Department of Energy and Process Engineering, NTNU, Kolbjørn Hejes vei 1B, Trondheim NO-7491, Norway

ARTICLE INFO

Keywords:
Gas separation
CCS
CO_2 capture
Exergy
Efficiency

ABSTRACT

A generic exergy targeting tool for gas separation processes is developed, which is applicable to any defined boundary conditions for incoming feed gas as well as delivered separation products. Whereas targeting tools in the literature so far are mostly simplified and limited to post-combustion related cases and isothermal and isobaric conditions, the present approach is based on a rigorous exergy methodology, which enables exergy targeting for a broad spectrum of boundary conditions.

Understanding the causes behind thermodynamic losses throughout the process is a prerequisite for improving energy efficiency. In this respect, exergy analysis provides a powerful tool, which enables the identification and quantification of irreversibilities and thereby exergy losses. The methodology is used to show that common separation processes can be attributed with negative minimum separation work, since a corresponding reversible separation process would yield an exergy output in addition to providing the specified product streams.

CO_2 capture involves considerable energy demand caused by the various processing steps. The exergy balance of a CO_2 capture process can in turn be applied to determine the exergy efficiency for each sub-process as well as for the overall process. Exergy efficiency criteria can be formulated in different ways, and in the present work it will be evaluated primarily against the minimum theoretical exergy requirement, that is, the performance theoretically achievable for a reversible process.

Through a quantitative example based on published literature on CO_2 separation from syngas, it is shown that a process may still require a substantial amount of exergy input despite having a negative minimum separation work, which in turn results in a negative exergy efficiency. A relation between sub-system exergy efficiency and overall system exergy efficiency is derived on a general basis. For the numerical example of CO_2 capture from syngas, the derived relation shows consistency and is able to reproduce the total process efficiency also when one of the sub-processes, CO_2 separation, has a negative exergy efficiency. Exergy efficiency results are finally compared with corresponding results based on a well-established rational exergy efficiency.

Despite different values and even signs for the separation sub-process efficiency, it is still shown that there are no contradictions between the two efficiency criteria when used consistently, since they give identical total exergy efficiency when applied to the control volume of the combined CO_2 separation and compression process, and since identical results are obtained also when expressing the total exergy efficiency as a linear combination of the two sub-process efficiencies, one of which has a negative sign.

1. Background and motivation

CO_2 capture processes are generally causing considerable energy demand that is related to most or all of the involved processing steps. Such steps include CO_2 separation and enrichment, drying and similar conditioning processes, compression and liquefaction. CO_2 enrichment and separation from flue gas, synthesis gas, tail gas or natural gas, and the conditioning to viable transport and storage conditions are inherently parasitic, thus contributing to, amongst others, energy-driven operational expenditures and thereby affecting the economy of CO_2 capture, whether this is intended for utilisation (CCU), permanent storage (CCS) or enhanced oil recovery (EOR). In the pursuit of improved and less parasitic CO_2 capture processes, it is of utmost importance to better understand the efficiency of capture processes and technologies, as well as the causes of inherent thermodynamic losses for different technologies. This insight can in turn reveal further improvement potentials, as

* Corresponding author.
E-mail address: david.berstad@sintef.no (D. Berstad).

https://doi.org/10.1016/j.ccst.2023.100111
Received 26 February 2023; Received in revised form 31 March 2023; Accepted 31 March 2023

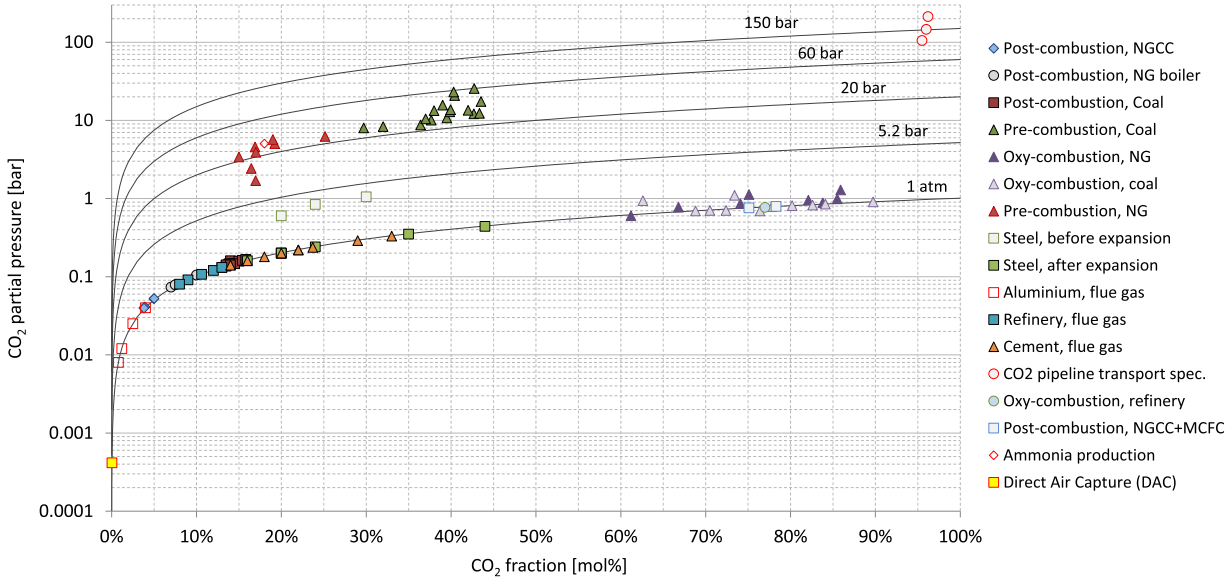

Fig. 1. Examples of capture conditions for natural and industrial CO_2 sources characterised by CO_2 molar fraction (horizontal axis) and CO_2 partial pressure (vertical axis). The plot is based on (Berstad et al., 2013) and amended with additional relevant examples.

well as identify limitations and barriers associated with a given technological solution.

Exergy analysis provides a powerful tool as a means for identifying and quantifying the thermodynamic losses, referred to as irreversibilities, on every level of a CO_2 capture process. Losses can be quantified individually for each component, locally for any defined sub-process control volume, as well as globally for the total process from feed to products. Furthermore, the performance can be formulated in different ways on the basis of various criteria for exergy efficiency. A fundamental approach in this respect is to relate the actual exergetic performance and irreversibilities of a process to what is theoretically achievable for a loss-free, reversible process.

CO_2 can in principle be captured from a multitude of natural and industrial/anthropogenic sources. Within this scope, the potential CO_2 capture conditions vary in a very broad sense. CO_2 capture conditions can be characterised by multiple intensive and extensive properties such as gas flowrate, temperature, pressure and chemical composition. Pressure level and chemical composition are two central properties in this respect, which can be used to calculate the CO_2 partial pressure in a gas stream. CO_2 partial pressure is a characterising property of high importance, and arguably the main property of interest when it comes to sorting and ranking the different CO_2 capture conditions found amongst the multitude of potential sources.

In the world of industrial research and development, CO_2 capture is targeted for a wide range of sources, from ambient air with an extremely low CO_2 partial pressure through Direct Air Capture (DAC) (Erans et al., 2022), to CO_2-rich, high-pressure synthesis gas from natural gas reforming (Oh et al., 2022) or coal gasification (Jordal et al., 2015). Across this span of capture conditions the CO_2 partial pressure and thus the available driving force for CO_2 separation varies by as much as five orders of magnitude, from around 0.4 mbar in the case of DAC to multiples of 10 bar in the case of synthesis gas derived from coal gasification (Berstad et al., 2013). Given these extreme differences as well as the realisation that each separation technology has inherent limitations and can perform efficiently only within certain ranges of CO_2 capture conditions, different technologies and solutions are required to cover the full spectrum of potential CO_2 sources (Berstad et al., 2013).

A diagram covering a considerable portion of the CO_2 capture spectrum is provided in Fig. 1. The plot shows several data points, each representing the capture conditions for a CO_2-containing gas in form of the characterising CO_2 molar fraction and CO_2 partial pressure. In addition, certain isobars for total pressure between 1 atm and 150 bar are plotted, including 5.2 bar, which is the approximate triple point pressure for pure CO_2, and which has relevance to separation processes utilising phase change such as CO_2 liquefaction or CO_2 anti-sublimation. In addition to source conditions, a handful of typical CO_2 pipeline transport conditions are plotted in the top right corner of the chart.

In addition to the plot providing an overview of capture conditions, another aspect is that qualitatively, the distance between the locations of any given CO_2 capture condition and the final transport condition can be interpreted as the difficulty or expected energy intensity of CO_2 separation and CO_2 compression combined. Capture conditions for DAC and other highly diluted CO_2-containing flue gases are located towards the bottom left corner and are those farthest away from pipeline transport conditions in the chart. These are generally encumbered with higher energy demands for CO_2 capture and compression than what is the case for high-pressure and high-concentration sources located closer to the transport state. In the following, this qualitative assessment will be developed into a strictly quantitative one by analysing capture and transport conditions through rigorous exergy analysis.

The goals of the present work are to apply rigorous exergy analysis in order to:

- Obtain a quantification method for the minimum theoretical exergy required to achieve separation of a CO_2-containing process stream into desired separation products, valid for any chosen states
- Obtain an analytical relation between the exergy efficiency of sub-processes and the total exergy efficiency for CO_2 capture processes, where the exergy efficiency is defined as the ratio between theoretical and actual exergy requirement

These methods and the complementary results that will be produced for relevant examples, will contribute to new insights, showing e.g. that:

- CO_2 separation sub-processes can in certain instances be attributed negative values for the minimum theoretical exergy requirement, as well as negative exergy efficiency
- The developed relation between the exergy efficiencies of the sub-process and that of the overall CO_2 separation and compression process is consistent, even when a negative sub-process efficiency is encountered

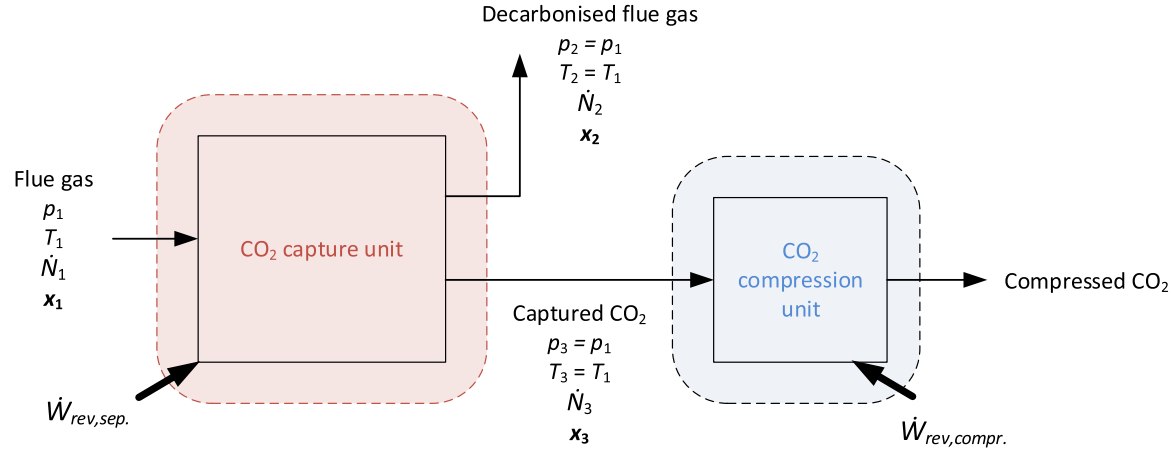

Fig. 2. Black box representation of CO_2 separation at isobaric and isothermal conditions and subsequent CO_2 compression.

2. Literature review of exergy calculations for isothermal and isobaric separation processes based on ideal gas assumptions

2.1. Targeting minimum theoretical separation work

The minimum theoretical separation work or minimum exergy requirements for separation is obtained when all processes are considered reversible. This minimum work has been derived for CO_2 capture under certain conditions in the published literature. It should be noted that the main focus in the literature is on isobaric and isothermal CO_2 separation in the sense that the respective temperatures and pressures of the incoming feed stream (T_1, p_1) and outgoing product streams (T_2, p_2 and T_3, p_3) are assumed to be equal as indicated in Fig. 2, while the composition vectors ($\boldsymbol{x_1}$, $\boldsymbol{x_2}$, $\boldsymbol{x_3}$) and molar flows ($\dot{N}_1$, $\dot{N}_2$, $\dot{N}_3$) are the only properties undergoing changes. This assumption can be reasonable as long as atmospheric or near-atmospheric pressure levels are considered, that is, conditions applicable to primarily post-combustion CO_2 capture and DAC.

These assumptions (constant temperature, constant pressure and ideal gas) allow for simplifications in the analytical derivation of the reversible separation work or exergy requirement $\dot{W}_{rev,sep.}$ of a CO_2 separation unit. Thermomechanical exergy terms for the feed and product streams balance each other, rendering chemical exergy as the only impacting terms. Moreover, since there are no net chemical reactions and there is otherwise a conservation of mass for each chemical component, the reversible separation work can be expressed as:

$$\dot{W}_{rev,sep.} = \bar{R}T_0\left[\dot{N}_2\sum_j x_{2,j}\ln x_{2,j} + \dot{N}_3\sum_j x_{3,j}\ln x_{3,j} - \dot{N}_1\sum_j x_{1,j}\ln x_{1,j}\right] \quad (1)$$

where the product stream flowrates ($\dot{N}_2$, $\dot{N}_3$) and chemical compositions ($\boldsymbol{x_2} = [x_{2,1}, x_{2,2}, \ldots, x_{2,j}]$, $\boldsymbol{x_3} = [x_{3,1}, x_{3,2}, \ldots, x_{3,j}]$) of each product stream is a function of the specified feed flowrate ($\dot{N}_1$), feed composition ($\boldsymbol{x_1} = [x_{1,1}, x_{1,2}, \ldots, x_{1,j}]$) and split ratio of each component (1, …, j) in the black-box separation process.

The expression may be further condensed by compounding all diluents (components other than CO_2) and assuming a binary ideal gas mixture made up of CO_2 and the complementary "non-CO_2" components. Another common approximation is to consider the captured CO_2 stream as pure (Herzog et al., 2009), which eliminates the mixing term for the CO_2 product stream from the expression since $\ln x_{3,CO2} = 0$ and every other value for $x_{3,j} = 0$. The absolute term for $\dot{W}_{rev,sep.}$ in Eq. (1) is commonly scaled with the flowrate of captured CO_2 (equals $\dot{N}_3 \cdot x_{3,CO2}$) so that the minimum separation work is expressed in specific terms, e.g. kJ/mol CO_2. In addition to different options for expressing Eq. (1), there are also different ways to derive and arrive at this result.

Wilcox (2012) derived the expression for minimum separation work based on the Gibbs free energy change between the feed stream and the two product streams. Underlying assumptions were constant temperature, constant total pressure and ideal gas behaviour. The same outline based on Gibbs free energy was made by Zhao et al. (2017). Rochedo and Szklo (2013) applied the same ideal gas-based relation for estimating the minimum work of separation (MWS) for absorption-based capture processes, given isothermal conditions. A second method, based on the Peng–Robinson equation of state, was also applied as a benchmark for the ideal gas model, but no further details on the exergy methodology were provided. Herzog et al. (2009) declared the same relation for the ideal work of separation in a rough minimum work calculation. Nord and Bolland (2020) showed different approaches to arrive at the same relation, for instance by considering the reversible work for compressing diluted gas components from their initial partial pressure, as also found in the theory of chemical exergy of mixtures outlined by Kotas (1995), and combining this with the chemical exergy balance of the black box separation process.

2.2. Quantifying the exergy efficiency of separation with minimum theoretical separation work as benchmark

2.2.1. Exergy efficiency definition

A commonly agreed expression for quantifying the exergetic performance of a post-combustion CO_2 separation process with isobaric and isothermal boundary conditions, is the ratio between minimum theoretical separation work, expressed from Eq. (1), and actual separation work:

$$\psi = \frac{\dot{E}_{in,\ min.\ th.}}{\dot{E}_{in,\ act.}} \quad (2)$$

In more general terms, since many processes have a combined exergy input in terms of both mechanical power and thermal energy, the terms for work or power can be replaced by exergy to represent the various forms of exergy input to the process. Hence, the symbol for power or rate of work $\dot{W}$ used in Eq. (1) can be substituted by the rate of exergy $\dot{E}$ as done in Eq. (2).

2.2.2. Exergy efficiency of chemical solvent-based post-combustion CO_2 separation

Nord and Bolland (2020) provided a numerical example for capturing 85% of CO_2 from a flue gas containing 14 mol% CO_2. A Monoethanolamine (MEA) process with a specific reboiler duty of 4 MJ_{th}/kg_{CO2} and a specific auxiliary power requirement of 0.04 MJ_p/kg_{CO2} was assumed as energy input. The resulting stand-alone exergy efficiency for an isobaric separation process was assessed to be

13–14%, whereby the exergy input from auxiliary steam was estimated from a heat-to-power conversion factor, based on the alternative use of steam in turbines.[1]

Amrollahi et al. (2011) assessed the exergy efficiency of a chemical solvent unit capturing 90% of CO_2 from gas turbine exhaust containing 3.8 mol% CO_2. With a specific reboiler duty of 3.86 MJ_{th}/kg_{CO2}, the resulting exergy efficiency was calculated to be 21.2%. The overall exergy efficiency for the separation and compression processes combined was 31.6%. For more advanced configurations of the capture unit, the stand-alone exergy efficiency could be increased to 25.0%, and the overall exergy efficiency for separation and compression correspondingly to 35.6% (Amrollahi et al., 2011).

Edwards et al. (2015) have assessed the typical stand-alone exergy efficiency of CO_2 capture processes by amine absorption to be around 20% based on process data from (Rochelle et al., 2011). Cao et al. (2017) conducted an exergy analysis of a chemical looping air separation (CLAS) IGCC plant with post-combustion CO_2 capture using MEA as chemical solvent. The exergy efficiency of the CO_2 capture and compression unit is reported to be 28.7%, but the applied definition of exergy efficiency is not corresponding to Eq. (2), rather as the ratio of total exergy output and input to the sub-process control volume. Other works in the literature have estimated the exergy losses/irreversibilities for CO_2 capture units (Ertesvåg et al., 2005; Geuzebroek et al., 2004; Feyzi et al., 2017), but they have not assessed the capture unit stand-alone exergy efficiency.

3. Method: outline and implementation of a generic exergy targeting tool for general boundary conditions

The simplified approach to obtain minimum separation work for a reversible separation process, as given by Eq. (1), has strict limitations and validity ranges. To further develop the methodology to cater for any chosen boundary conditions, the basis for a generic exergy targeting framework is presented. The purpose is to enable reversible targets for any pressure level, temperature level, chemical composition and phase for any given separation. The model is entirely based on freely defined stream conditions and can be implemented in simulation software using any chosen thermophysical fluid property model. As will be illustrated later in Section 5, this targeting approach is necessary for enabling the evaluation of exergetic performance of common CO_2 separation technologies for which there are substantial changes in e.g. pressure level between feed and products.

The steady-state exergy balance of an open control volume (CV) with any number of streams crossing the boundaries, can be expressed as follows (Kotas, 1995):

$$0 = -\dot{W}_{cv} + \sum_{i,\ \text{in}} \dot{N}_i \bar{e}_i - \sum_{j,\ \text{out}} \dot{N}_j \bar{e}_j + \sum_r \dot{Q}_r \left(1 - \frac{T_0}{T_r}\right) - \dot{I}_{cv} \tag{3}$$

where the term $\dot{W}_{cv}$ is the exergy transfer rate in the form of work crossing the boundary (negative sign for work entering the control volume), $\dot{I}_{CV}$ is the rate of irreversibility in the control volume and $\dot{Q}_r$ are individual heat flows (positive sign for heat entering the control volume) occurring at temperature level T_r. The factor $(1 - T_0/T_r)$ denotes the dimensionless exergetic temperature of heat flow $\dot{Q}_r$. $\dot{N}_i$ and $\dot{N}_j$ are the individual inlet and outlet molar flowrates while the terms $\bar{e}_i$ and $\bar{e}_j$ denote the molar exergy for each flow of matter, which can be further decomposed into:

$$\bar{e} = \bar{e}^{tm} + \bar{e}^{ch} + \bar{e}^{kin} + \bar{e}^{pot} \tag{4}$$

for the present purpose, the change in molar kinetic exergy $\bar{e}^{kin}$ and potential exergy $\bar{e}^{pot}$ are negligible and considered to be at substantially lower orders of magnitude compared to thermomechanical exergy $\bar{e}^{tm}$ and chemical exergy $\bar{e}^{ch}$. Molar thermomechanical exergy is defined as:

$$\bar{e}^{tm} = \bar{h} - \bar{h}_0 - T_0(\bar{s} - \bar{s}_0) \tag{5}$$

where $\bar{h}_0$ and $\bar{s}_0$ denote the molar enthalpy and entropy at ambient conditions, that is, at ambient temperature T_0 and ambient pressure p_0. In this work T_0 is generally set to 288 K, with the exeption of certain numerical examples using 298 K in Sections 3.1, 3.2 and 5.7, while p_0 is always equal to 1.013 bar. Chemical exergy for a multicomponent stream of matter on a molar basis can be expressed as (Voldsund et al., 2014):

$$\bar{e}^{ch}_{mix} = \sum_j x_j \bar{e}^{ch}_j + \bar{h}_0 - \sum_j x_j \bar{h}_{j,0} - T_0 \left(\bar{s}_0 - \sum_j x_j \bar{s}_{j,0} \right) \tag{6}$$

where x_j is the molar fraction of component j, $\bar{e}_j^{ch}$ is the molar chemical exergy of component j and $\bar{h}_{j,0}$ and $\bar{s}_{j,0}$ are the molar properties for enthalpy and entropy, respectively, at ambient conditions for component j in pure form.

In separation processes with no net chemical transformations[2] and thus a conservation not only of mass but also the number of molecules for each single component, the flowrate for each single chemical component balances. Consequently, the amount of chemical exergy for each component in pure form also balances and the first term on the right-hand side of Eq. (6) can therefore be eliminated from the exergy balance.

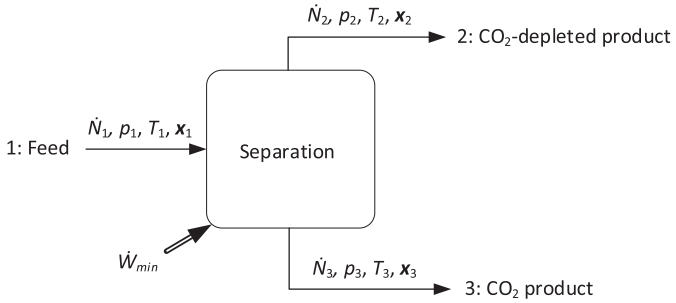

Fig. 3. Generic control volume for a reversible gas separation process.

Fig. 3 illustrates a reversible CO_2 separation process where a feed stream enters at molar flowrate $\dot{N}_1$, thermodynamic state 1 (p_1, T_1) and with composition vector $\boldsymbol{x}_1$. In the black box for the separation process, this feed stream is split into two product streams: a CO_2-depleted product at thermodynamic state 2 with properties $\dot{N}_2$, p_2, T_2 and $\boldsymbol{x}_2$ and a CO_2 product with properties $\dot{N}_3$, p_3, T_3 and $\boldsymbol{x}_3$. No other process streams are assumed to enter or leave the boundaries, although the model may be extended to any number of product streams, as well as feed streams if required. Assuming reversible separation, while using arrows rather than sign convention where work produced by the system in the control volume is positive, the expression for minimum theoretical separation work can be expressed as:

$$\dot{W}_{min} = \dot{N}_2(\bar{e}_2^{tm} + \bar{e}_2^{ch}) + \dot{N}_3(\bar{e}_3^{tm} + \bar{e}_3^{ch}) - \dot{N}_1(\bar{e}_1^{tm} + \bar{e}_1^{ch}) \tag{7}$$

Eq. (7) can be modified by scaling the minimum theoretical separation work with the molar flowrate of the captured/separated CO_2 in order to obtain an expression for specific work requirement in kJ/mol CO_2 separated:

$$\bar{w}_{min} = \frac{\dot{N}_2(\bar{e}_2^{tm} + \bar{e}_2^{ch}) + \dot{N}_3(\bar{e}_3^{tm} + \bar{e}_3^{ch}) - \dot{N}_1(\bar{e}_1^{tm} + \bar{e}_1^{ch})}{x_{CO2,3}\dot{N}_3} \tag{8}$$

[1] The exergy efficiency will drop to around 11 % if the Eq. (2) criterion is applied, whereby the thermomechanical exergy transferred from steam condensation is considered as exergy input instead of the alternative steam turbine output.

[2] With respect to streams crossing the control volume boundaries, thus independent of any intermediate chemical transformations inside the control volume e.g. through chemical sorption.

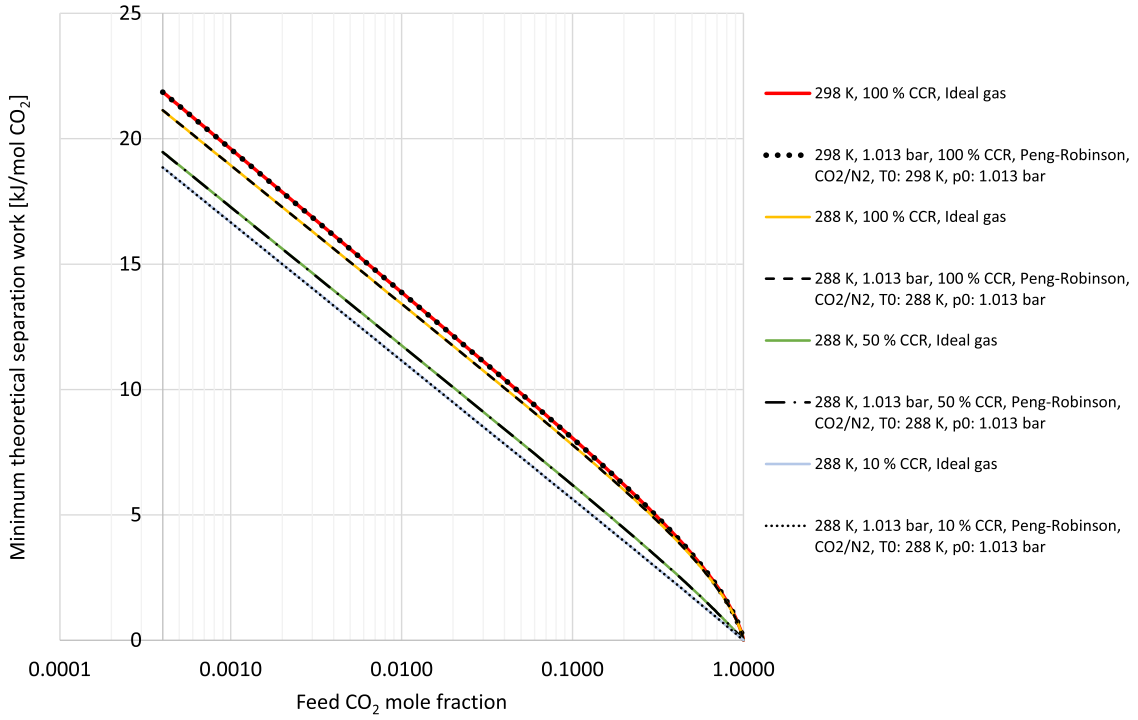

Fig. 4. Comparison of minimum theoretical work for different isothermal and isobaric separations.

3.1. Comparison of exergy targeting results for ideal gas-based and rigorous exergy calculations

The dominant air components nitrogen and oxygen exert ideal gas characteristics at temperature and pressure in the proximity of ambient conditions. This can be a reasonable approximation also for CO_2, which has a compressibility factor of around 0.994–0.995 in the range 288–298 K at atmospheric pressure. Based on the ideal gas-based expression in Eq. (1), minimum theoretical separation work has been quantified for four arbitrarily selected combinations of constant temperature and CO_2 capture ratio (CCR):

1 100% CCR at 298 K
2 100% CCR at 288 K
3 50% CCR at 288 K
4 10% CCR at 288 K

The purpose of this selection of combinations is to show the variation in results for a high (100%), medium (50%) and low (10%) CCR for a given T_0 (288 K), and to show the impact of T_0 (298 K vs. 288 K) for a fixed CCR (100%). For all four combinations, the CO_2 product is assumed to be pure, and the full spectrum of CO_2 fractions in the feed has been considered, from 400 ppm to 1. For each case, the minimum theoretical separation work is plotted in Fig. 4 as function of feed CO_2 fraction and scaled by the molar flowrate of captured CO_2.

The exergy targeting model derived from Eqs. (3)–(8) has been implemented in the process simulation software Aspen HYSYS. To compare results, the four separation cases above, quantified using ideal gas relations, have been reproduced with the implemented model. Whereas the ideal gas-based calculation requires only ambient temperature as well as mole fractions and flowrates for each process streams as input, the simulation model requires additional specifications:

- Feed and product stream temperatures and pressures
- Both ambient temperature and pressure in order to quantify ambient state properties for the feed stream and product streams, as well as for pure components
- Thermophysical property model

For all four simulation cases, the ambient pressure is set to 1.013 bar. The constant separation temperature as well as ambient temperature are set equal to that specified in each ideal gas-based calculation. The Peng–Robinson equation of state has been used to calculate thermophysical fluid properties. Comparisons made in Fig. 4 shows very high consistency between the two calculation approaches and such corroborates the validity of the ideal gas models for the present conditions.

3.2. Limitations of ideal gas-based exergy targeting methods and the need for universal methods

The close match between the results using the ideal gas model and the Peng–Robinson equation of state shown in Fig. 4 is explained by the fact that the gas constituents, to a large extent also CO_2, exert ideal gas behaviour at the given temperature and pressure levels. For other conditions, however, the ideal gas assumption may become significantly less accurate and lead to considerable errors in exergy calculations and thus in estimates of minimum separation work.

As one illustrative example where simplified approaches may cause inaccurate estimates, Wilcox (2012) presents the same type of diagram for reversible separation as that shown in Fig. 4. In Wilcox (2012), ideal gas-based estimates for reversible separation work at constant pressure and temperature (two isotherms: 298 K and 338 K) are plotted for all CO_2 feed fractions between ca. 400 ppm and 1. In this plot, CO_2 fractions in the interval 40–60% are indicated to represent conditions typical for integrated gasification combined cycles (IGCC). While this certainly is the case for the CO_2 fraction, the absolute pressure levels relevant for IGCC are considerably higher than pressures for which ideal gas behaviour is a reasonable approximation. For pressure levels relevant for shifted IGCC syngas, typically 25–70 bar (Berstad et al., 2013), properties such as compressibility deviate considerably from ideal gas assumptions. This applies for CO_2 in particular, with a critical point of about 31 °C and 73.8 bar. Non-ideal characteristics contribute to invalidating the ideal gas basis, which ignores the actual pressure level.

To exemplify the magnitude of expected deviations in minimum separation work between the ideal gas-based estimates and calculations based on thermodynamic state properties for approximated IGCC con-

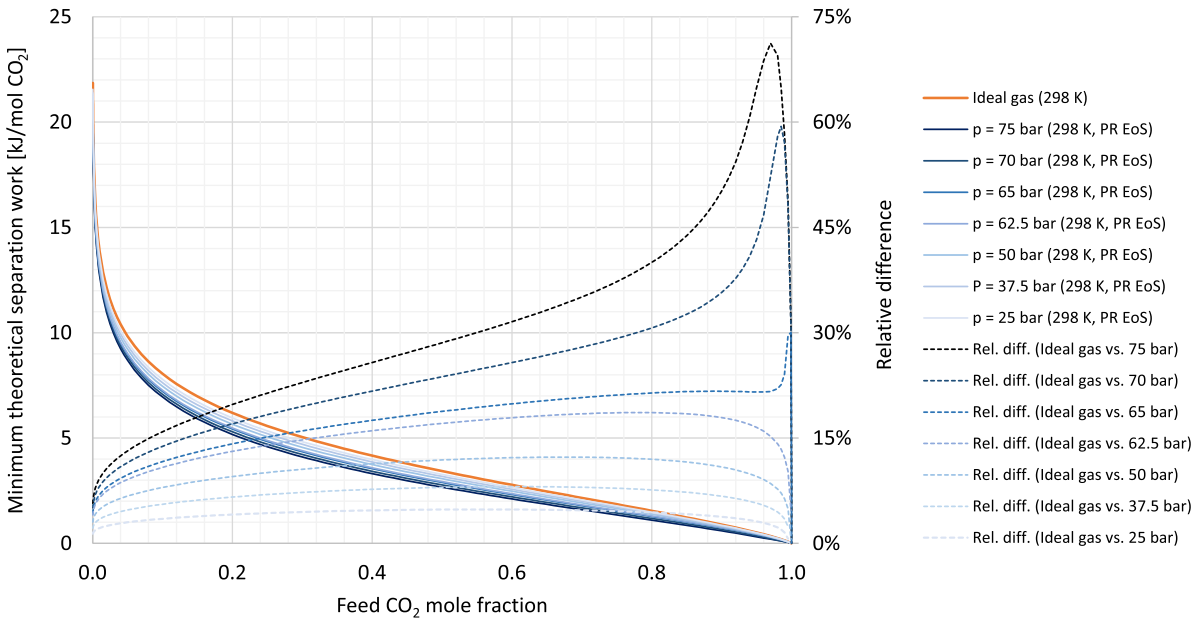

Fig. 5. Estimates for reversible isothermal (298 K) and isobaric separation work for 100% CCR for ideal gas mixtures, as well as for binary H_2/CO_2 mixtures at different pressure levels using Peng–Robinson EoS for thermophysical properties. Ambient temperature and pressure are set to 298 K and 1.013 bar, respectively. CO_2 products are assumed to be pure.

ditions, consider Fig. 5. This diagram shows the minimum separation work for isothermal (298 K) and isobaric separation from the ideal gas-based expression in Eq. (1), compared to simulation results for binary CO_2/H_2 mixtures based on Eq. (8) and the Peng–Robinson equation of state for the pressure levels between 25 bar and 75 bar.

As can be observed from the group of curves, the minimum separation work for isothermal and isobaric conditions decreases with pressure level. Relative deviations approach zero in the extreme ends of the scale where the feed CO_2 fraction approaches either 0 or 1 and culminate at a maximum value between these extremes. For CO_2 fractions typical for shifted syngas in IGCC applications, which corresponds to the rough x-axis interval of 30–60 mol%, the deviations between the two models (ideal gas versus simulations using Peng–Robinson) are found to be up to approximately 5% for 25 bar, 12% for 50 bar and 32% for 75 bar.

Whereas the isothermal and isobaric ideal gas calculation models only account for the change in chemical exergy from feed to products, the model misses out on possible changes in thermomechanical exergy since ideal gas implies zero enthalpy of mixing. When the total thermomechanical exergy remains unchanged between feed and product states, it is consequently eliminated from the balance. Even for isobaric and isothermal conditions, Fig. 5 illustrates that the error in targets for minimum exergy requirement can become considerable.

Generic exergy targeting becomes even more important when moving from isothermal and isobaric conditions at low pressure, to assessing separation processes where the boundary stream conditions in form of temperature, pressure and potentially phase can change considerably. As will be discussed in Section 5 through numerical examples, the fundamental understanding of minimum exergy requirement is a prerequisite for further evaluation of the exergy efficiency for separation processes with such characteristics.

4. Method: relation between exergy efficiency of sub-processes and overall system exergy efficiency

As outlined in Section 2.2, the common definition of exergy efficiency is defined as the ratio between minimum theoretical exergy requirement and the actual exergy requirement, as given by Eq. (2). A typical CO_2 capture process consists of two consecutive stages of processing:

1 Separation of CO_2 from a gas mixture
2 Compression of the enriched CO_2 product

The exergy efficiency of each processing stage can be evaluated from the generic Eq. (2) criterion. Similarly, if the system boundary is drawn around both sub-processes, the overall exergy efficiency of the combined process can still be quantified by the same criterion. The intention of the present section is to derive a general relation between each subsystem's exergy efficiency and that of the overall system. The relation is intended to be general in the sense that it is valid for more complex process configurations beyond the typical two-stage, sequential separation and compression process. Moreover, it will be used to verify the exergy efficiency figures in numerical examples analysed in Section 5.7.

An example of an arbitrary and somewhat more complex process configuration is shown in Fig. 6, and consists of three sub-processes, I–III. Two material streams enter the control volume of sub-process I, one feed stream with exergy flow $\dot{E}_1$ and a recycled stream from sub-process II, with corresponding exergy flow $\dot{E}_{REC}$. Two product streams leave the boundary of sub-process I. One of the outlet streams, with exergy flow $\dot{E}_2$, is sent to sub-process II, which in turn produces two material streams with respective exergy flows $\dot{E}_3$ (leaving the overall system) and $\dot{E}_{REC}$ (flowing back to sub-process I). The other product stream from sub-process I has exergy flow $\dot{E}_4$ and enters sub-process III, which in this example has only a single product stream leaving the system with exergy flow $\dot{E}_5$. Although not necessary for the development of mathematical relations, it could be useful for the reader to lower the abstraction level by suggesting what each sub-process in Fig. 6 could represent. One out of many such possible sets of process abstractions *could be*:

- I: CO_2 main separation process in form of using a solvent.
- II: Process for additional separation and enrichment of CO_2 not captured in sub-process I. This could be a membrane paired with recompression of CO_2-enriched permeate, which is recycled to the main separation in sub-process I.
- III: Compression of captured CO_2.

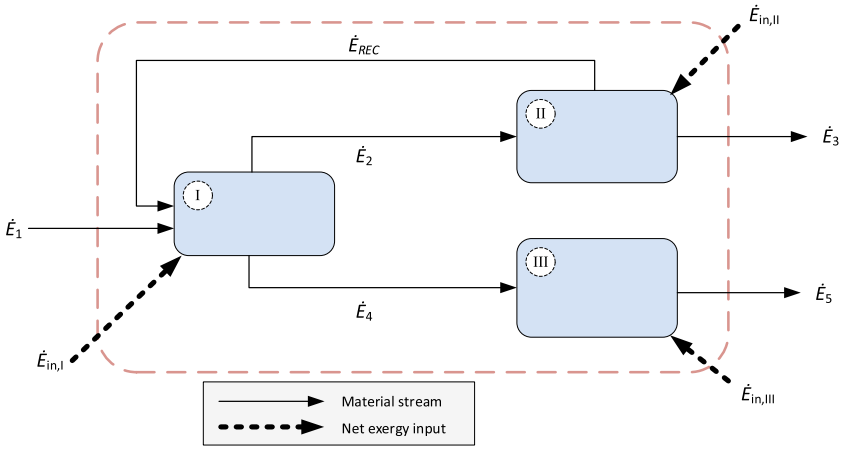

Fig. 6. Control volume and exergy flows for a process made up of sub-processes I, II and III.

The control volume enclosing each sub-process has a net auxiliary exergy input, denoted $\dot{E}_{in,I}$, $\dot{E}_{in,II}$ and $\dot{E}_{in,III}$, with positive sign in the direction of the dashed arrows. These represent the overall exergy flows associated with transfer of mechanical (work) and/or thermal energy (heat). Heat transfer can be direct or by means of a utility material stream such as steam that de-superheats and condenses, and thereby rejects heat to the control volume. In the case of a steam utility, the net mass flow into the control volume is zero and there is no mixing between the steam/water flow and the other material streams. In the case of direct steam injection, an additional process stream must be added to the mass balance.

Using the definition of exergy efficiency from Eq. (2), the exergy efficiency for the overall process in Fig. 6, enclosed by the dashed boundary line, is expressed as the ratio between the minimum theoretical exergy input, defined as the difference in exergy between the product and feed streams, and the actual net exergy input required to obtain the specified product streams:

$$\psi = \frac{\dot{E}_3 + \dot{E}_5 - \dot{E}_1}{\dot{E}_{in,I} + \dot{E}_{in,II} + \dot{E}_{in,III}} \tag{9}$$

Further, by both adding and subtracting the internal exergy streams $\dot{E}_2$, $\dot{E}_{REC}$ and $\dot{E}_4$ to/from the numerator, Eq. (9) can be transformed to:

$$\psi = \frac{\left(\dot{E}_3 - \dot{E}_2 + \dot{E}_{REC}\right) + \left(\dot{E}_5 - \dot{E}_4\right) + \left(\dot{E}_2 + \dot{E}_4 - \dot{E}_1 - \dot{E}_{REC}\right)}{\dot{E}_{in,I} + \dot{E}_{in,II} + \dot{E}_{in,III}} \tag{10}$$

Each numerator term enclosed by brackets corresponds to the minimum theoretical exergy requirement for the sub-processes I, II and III. Eq. (10) can thus be reformulated to:

$$\psi = \frac{\dot{E}_{in,\ min.\ th.,I} + \dot{E}_{in,\ min.\ th.,II} + \dot{E}_{in,\ min.\ th.,III}}{\sum_{i=I}^{III} \dot{E}_{in,i}} \tag{11}$$

Finally, by replacing each numerator term with the sub-process stand-alone exergy efficiency ψ_i, as defined in Eq. (2), the relation between overall system exergy efficiency and stand-alone sub-process efficiencies is a linear combination and can be expressed as:

$$\psi = \frac{1}{\sum_{i=I}^{III} \dot{E}_{in,i}} \cdot \sum_{i=I}^{III} \left(\psi_i \cdot \dot{E}_{in,i}\right) \tag{12}$$

It can be analytically derived a priori, as well as numerically verified a posteriori, that the relation arrived at in Eq. (12) applies also to a system made up of a general number of sub-processes ($i = 1, n$). The applicability of the relation will be further demonstrated in Section 5.7, suggesting that it is valid also for sub-processes with negative exergy efficiency ψ_i according to the definition in Eq. (2).

5. Results and discussion: exergy analysis to quantify the exergy efficiency of CO_2 removal from a high-pressure synthesis gas by chemical solvent scrubbing

In the following, an analysis of the stand-alone and overall exergy efficiency of a pre-combustion CO_2 capture case is conducted. The analysis of a quantitative example is necessary in order to provide further insight into the exergetic performance. To establish a numerical case exemplifying a typical exergetic performance of Methyl diethanolamine (MDEA) for CO_2 removal from syngas, process data has been adopted from Moioli et al. (2016; 2017). These references provide transparent process data that can be analysed by the exergy targeting methodology presented here.

5.1. Process description

The process structure for the CO_2 separation and subsequent compression process with boundary stream conditions are illustrated in Fig. 7 (partly reproduced from (Moioli et al., 2017)). A shifted and desulphurised stream of syngas originating from air-blown gasification enters an absorption column at 29.15 bar pressure. CO_2 is absorbed by a 50 wt% MDEA solution and subsequently released in two stages. CO_2 is partially desorbed in a flash stripper at 1.1 bar and thereafter in a stripping section where the solvent is regenerated by reboiler heat supplied through de-superheating and condensation of superheated steam supplied at 188 °C and 2 bar. The overall CO_2 capture ratio from the syngas stream is 95%. The two streams of released CO_2 leave the capture section at a pressure level equal to or slightly lower than 1.1 bar. Furthermore, the CO_2 is assumed to be pure, although it will be saturated with a minor fraction of water upon discharge. The water balance of the system, however, will have very low impact on the estimate for minimum theoretical separation work. Other minor simplifications made in this analysis are the omission of a minor solvent slip stream and a balancing solvent make-up stream, as well as disregarding trace impurities of H_2S, as the influence on exergy calculations is negligible.

With the boundary-crossing streams defined, the minimum theoretical exergy requirement can be calculated with the exergy targeting tool. It should be reiterated that the calculation of minimum exergy requirement is path-independent and requires only the defined boundary conditions as input and therefore, does not depend on the actual processing path. Stream data as well as estimated exergy flows are summarised in Table 1, based on Peng–Robinson for thermophysical properties. An initial observation which can be made is that the flow of chemical exergy as defined in Eq. (6) increases from 694.1 MW in the feed stream to a total of 705.4 MW for the two separation products combined. The separation process adds about 11.3 MW of chemical exergy and valorises the

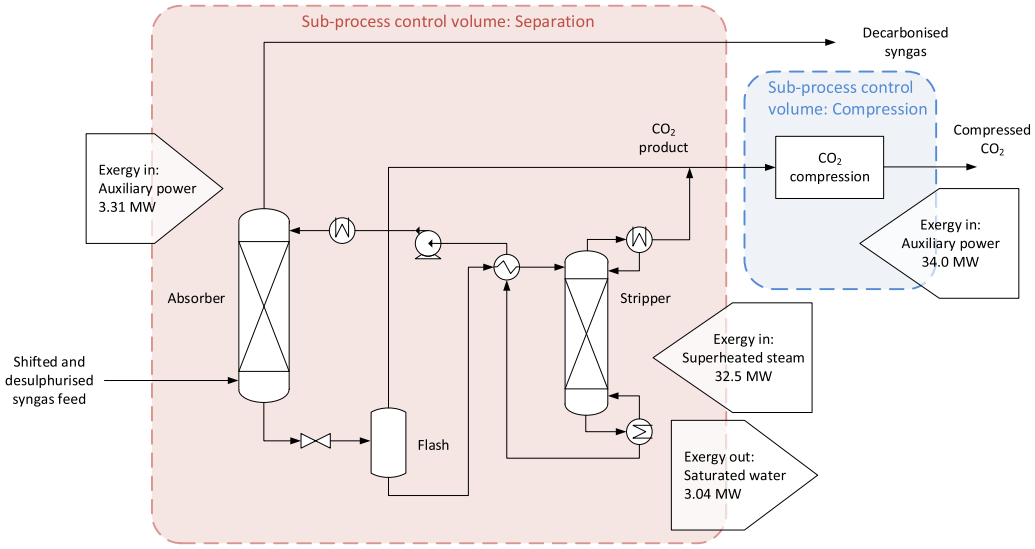

Fig. 7. Process structure, control volume and boundary-crossing exergy streams (material streams, power and thermal utilities) for the MDEA scrubbing process. Partly reproduced from Moioli et al. (2017).

Table 1
Chemical composition, flowrate and thermodynamic state of the syngas feed stream and separation product streams. Stream data is compiled from Moioli et al. (2016) and Moioli et al. (2017) with minor modifications. Exergy terms are calculated based on $T_0 = 288$ K, $p_0 = 1.013$ bar. 95% of CO_2 contained in the syngas feed stream is captured.

		Syngas feed	Decarbonised syngas	CO_2 product	Compressed CO_2
Mass flowrate	kg/s	232.86	133.78	99.08	99.08
Molar flowrate	kmol/s	9.388	7.137	2.251	2.251
Pressure	bar	29.15	29.15	1.10	110
Temperature	°C	44	45	30	30
Chemical composition					
N_2	mol%	44.98%	59.17%	0%	0%
CH_4	mol%	0.42%	0.55%	0%	0%
H_2O	mol%	0.19%	0.25%	0%	0%
H_2	mol%	27.86%	36.64%	0%	0%
CO_2	mol%	25.24%	1.66%	100%	100%
CO	mol%	0.78%	1.02%	0%	0%
Ar	mol%	0.53%	0.70%	0%	0%
Molar thermomechanical exergy	kJ/mol	8.02	8.08	0.211	8.91
Thermomechanical exergy flow	**MW**	**75.301**	**57.658**	**0.475**	**20.061**
[(a)] $\sum_j x_j \bar{e}_j^{ch}$	kJ/mol	76.70	94.75	19.48	19.48
[(b)] $\bar{h}_0 - \sum_j x_j \bar{h}_{j,0} - T_0(\bar{s}_0 - \sum_j x_j \bar{s}_{j,0})$	kJ/mol	−2.76	−2.06	0	0
Molar chemical exergy [(c)]	kJ/mol	73.93	92.69	19.48	19.48
Chemical exergy flow	**MW**	**694.089**	**661.502**	**43.855**	**43.855**
Total exergy flow (tm+ch)	**MW**	**769.390**	**719.160**	**44.329**	**63.915**

[(a)] First term in Eq. (6). Sum of fraction-weighted chemical exergy for pure components.
[(b)] Second term in Eq. (6). Mixing term.
[(c)] Sum of first and second term in Eq. (6).

two product streams in this respect. This increase in chemical exergy can also be calculated from the chemical mixing terms and molar flowrates only, as the first term in Eq. (6) for fraction-weighted chemical exergy for pure components, is eliminated when inserted in Eq. (7) or Eq. (8). It can also be verified that the increase in chemical exergy is otherwise in accordance with what can be estimated from the simplified expression in Eq. (1), which also gives 11.3 MW if the stream data from Table 1 is used as input, using $T_0 = 288$ K as temperature input.

Although providing quantified estimates for changes in chemical exergy, neither of the expressions in Eq. (1) or Eq. (6) are sufficient to determine the minimum exergy requirement when the boundary conditions involve changes in thermomechanical exergy. As can be observed from Table 1, the thermomechanical exergy rate for the inlet feed stream is 75.3 MW while the corresponding number for the separation products combined equals 58.1 MW. It can thus be ascertained that while the chemical exergy rate *increases* by 11.3 MW, the thermomechanical exergy rate *decreases* by 17.2 MW due to the low thermomechanical exergy in the low-pressure CO_2 product.

5.2. Interpretation of negative reversible separation work

It is established that the sub-process for CO_2 separation from the syngas, given the boundary condition applicable for the process, has a minimum theoretical exergy requirement with negative sign. The theoretical exergy requirement, which applies to a reversible process, subject to the given boundary stream conditions are:

- $\dot{W}_{min} = -5.90$ MW in absolute terms from Eq. (7)
- $\bar{w}_{min} = -2.62$ kJ/mol$_{CO2}$ in molar terms from Eq. (8)

The interpretation of this result is that a reversible process, although not realisable in practice, delivers the product streams at specified boundary conditions plus an additional exergy (e.g. power) output. This

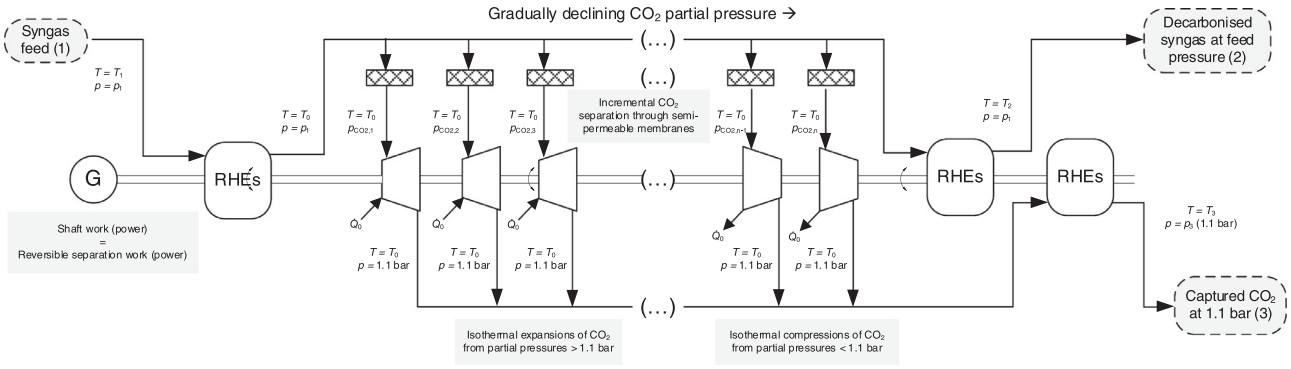

Fig. 8. Diagram for reversible separation of CO_2 through sequential and incremental separation by semi-permeable CO_2 membranes. Each incremental amount of separated CO_2 is brought to a target pressure (1.1 bar) by either isothermal expansion or compression at T_0.

must not be confused with the notion of expecting a real separation process to deliver anything close to such a performance, but it serves as a rigorous reference based on which the actual exergetic performance of the process can be evaluated, in the same way the classical post-combustion capture processes exemplified in Section 2.2 are evaluated. The negative sign is provided by performing the exergy calculations for the control volume, based on the properties of the process streams crossing the system boundaries. Although the calculations of reversible separation work are independent of the actual process taking place inside the control volume, it is possible to provide different abstractions of reversible processes as explanations as to why a reversible benchmark process would deliver a net exergy output.

5.3. Process abstractions for reversible separation

To provide an alternative angle complementing the sole equation-based calculation of reversible separation work, and to further illustrate why minimum separation work can take negative values, a similar approach can be taken as that by Kotas (1995). Fig. 8 shows a process diagram where a reversible separation of CO_2 from the high-pressure syngas is achieved, and where the separated CO_2 is delivered at its defined target pressure of 1.1 bar. The feed stream is first brought from supply temperature to ambient temperature T_0 through heat rejection to a sequence of reversible power-generating heat engines (RHEs), which in turn contribute to the power generation of the shaft to which they are connected. Thereafter, CO_2 gradually separates selectively from the gas mixture through a sequence of semi-permeable membranes, where the permeate pressure of each stage equals the local CO_2 partial pressure.

The description and methodology differ somewhat from that in Kotas (1995) since unlike the ambient surroundings, there is no "endless supply" (Sato, 2004) of components in the material feed stream. Whereas removing a substantial amount of oxygen, nitrogen or any other reference component from the air does not affect the reference conditions through depletion, the chemical composition of the syngas stream is continuously affected as CO_2 is removed. Therefore, the CO_2 partial pressure is strictly declining for each incremental semi-permeable membrane stage. Each fraction of separated CO_2 is retained at the local partial pressure at which it is available on the feed side of the incremental membrane stage, and at ambient temperature T_0. Each fraction of CO_2 is subsequently brought to the final target pressure (1.1 bar) either through isothermal expansion or compression. For any pressure level above target, expansion applies and conversely, compression applies for any permeate pressure below target.

After separation, both product streams are brought to their respective defined outlet temperatures, again by sequences of incremental reversible heat engines. In this particular case the RHEs downstream of the separation are actually reversible heat pumps, since the discharge temperatures are above T_0, and therefore draw a certain amount of power from the shaft. The net shaft work then equals the reversible separation work for the overall process.

Another reversible process abstraction can be made in which the changes in thermomechanical exergy and chemical exergy are decomposed to separate shafts. In the abstraction shown in Fig. 9, the feed stream is brought to ambient temperature as well as ambient pressure before the incremental separation of CO_2 in sequential semi-permeable membranes. Unlike the scheme in Fig. 8, where CO_2 partial pressures are both above and below target pressure, all partial pressures are below ambient pressure p_0, and all separated fractions of CO_2 are subsequently compressed isothermally to ambient pressure. After separation, including bringing all fractions of CO_2 to ambient pressure, the two product streams are available at ambient state T_0, p_0. Since this is also the state of the feed stream immediately upstream the CO_2 separation, the work (power) required to compress CO_2 reversibly from partial pressures to ambient pressure, equals the change in chemical exergy provided by the process. In the process diagram, these reversible and isothermal compressors are connected to a single shaft, to which the input work (power) equals the chemical exergy increase. All other reversible expanders, compressors and heat engines/pumps are connected to an additional shaft, the output work (power) of which equals the change in thermomechanical exergy. After separation, both product streams are brought to their respective defined outlet states, first by isothermal compression and thereafter by sequences of reversible heat engines. Whereas the net exergy requirement for the separation process equals the net work (power) of the single shaft in the process abstraction in Fig. 8, the corresponding exergy requirement equals the net work (power) of the two shafts in the Fig. 9 abstraction.

It should be mentioned that a third process abstraction is possible, where the changes in exergy are decomposed into three different shafts. In this abstraction, the changes in thermomechanical exergy would be split into what can be defined as temperature-based and pressure-based exergy components (Kotas, 1995), by separating compressor/expanders operating above ambient pressure to a dedicated shaft and correspondingly the reversible heat engines/pumps to another shaft.

5.4. Marginal and cumulative exergy requirement for reversible separation

In the process abstraction in Fig. 8, the first CO_2 molecule is reversibly separated and retained at the initial CO_2 partial pressure in the syngas. Consequently, it is therefore attributed the lowest marginal exergy requirement. On the other hand, the last CO_2 molecule to be separated has the highest exergy requirement, since the CO_2 partial pressure is strictly decreasing and eventually approaching zero. Therefore, the marginal reversible separation work for CO_2 is strictly increasing as the syngas is depleted of CO_2. This can be observed in Fig. 10 in which the blue-coloured curve represents the marginal reversible work for capturing and delivering CO_2 at 1.1 bar target pressure. The lowest value

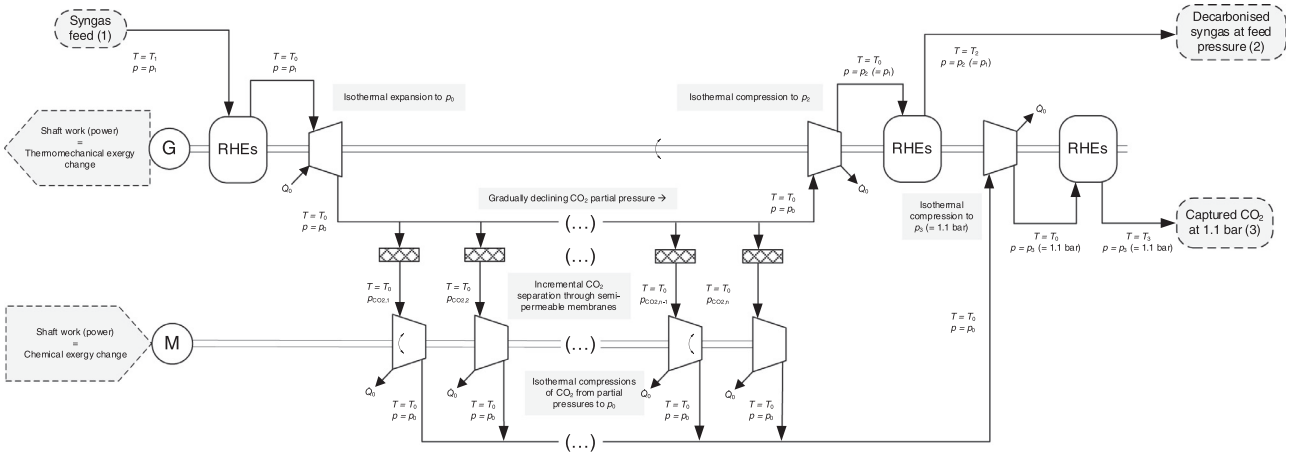

Fig. 9. Alternative process abstraction for reversible CO_2 separation where overall changes in thermomechanical and chemical exergy are decomposed and allocated to separate shafts.

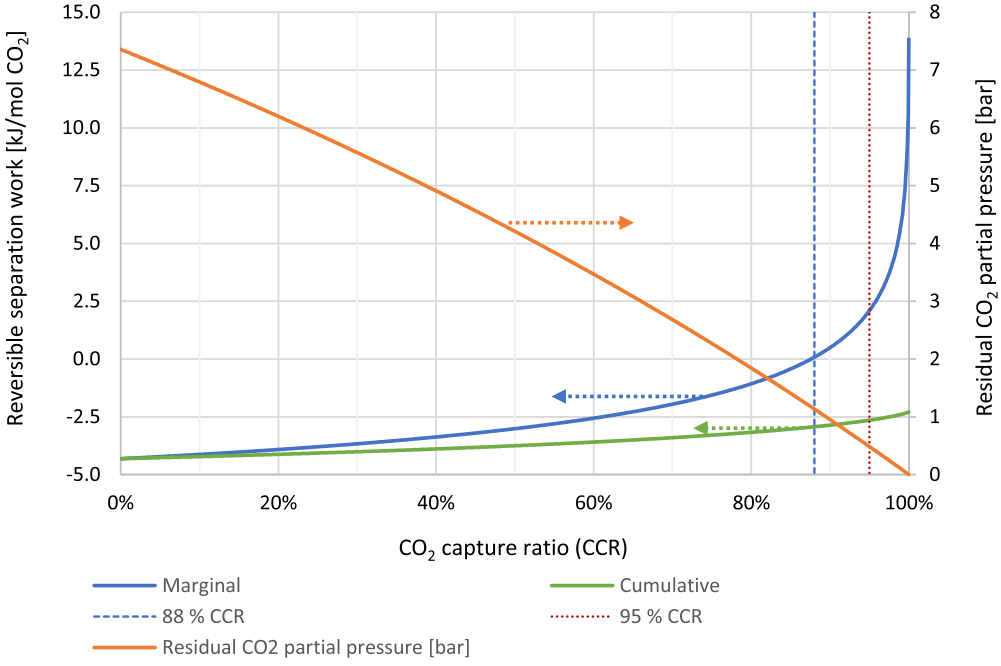

Fig. 10. Relation between CO_2 capture ratio and reversible separation work as well as residual CO_2 partial pressure for the syngas composition and boundary conditions given in Table 1.

occurs on the left-hand side, where the first CO_2 molecules are reversibly separated, and increases strictly when CCR increases, and sharply so as CCR approaches 100% and as the residual CO_2 partial pressure in the feed gas, represented by the orange-coloured curve, approaches zero. In the process abstraction in Fig. 8, the last molecules will thus permeate through the membrane at extremely low partial pressure, which in turn implies that the isothermal compression work, and therefore the marginal reversible capture work, will be extremely high.

Fig. 10 includes a dashed vertical line marking the CCR value equal to 88%. At this x-axis value, two observations can be made with respect to the Fig. 8 process abstraction:

- The residual CO_2 partial pressure approaches 1.1 bar from above and descends below this level for any further increase in CCR
- The marginal reversible separation work breaks the zero mark from below, and changes sign from negative to positive for further increase in CCR

This concurrence can be understood from and explained by the process abstraction in Fig. 8. The molecules captured when CCR is in the proximity of 88% permeate through the membrane and are retained at a pressure equal to the target pressure. Consequently, these molecules are passed on without requiring any changes in pressure by compression or expansion, and this fraction of CO_2 is therefore assigned a marginal reversible separation work equal to zero. From 88% CCR and upwards, any further amount of separated CO_2 requires compression up to target pressure and are therefore assigned marginal reversible capture work greater than zero.

The green-coloured curve in Fig. 10 indicates the cumulative value for reversible separation work, that is, the average molar reversible separation work for all molecules captured up to any given x-axis value for CCR. As stated in Section 5.2, the exergy targeting model gives –2.62 kJ/mol_{CO2} as reversible molar separation work for 95% CCR. This value is indicated with a second dashed vertical line. For the cumulative curve, the y-axis value at x-axis value CCR = 95%, is equal to –2.62 kJ/mol_{CO2}. Since the marginal reversible separation work is strictly

Table 2
Exergy balance for the sub-process control volume of the CO_2 separation process.

Inlet exergy streams	Shifted synthesis gas exergy flow	MW	769.4
	Superheated steam exergy flow	MW	32.5
	Auxiliary power exergy flow	MW	3.31
	Sum, inlet exergy flow	**MW**	**805.2**
Outlet exergy streams	Decarbonised synthesis gas exergy flow	MW	719.2
	CO_2 product exergy flow	MW	44.3
	Saturated water exergy flow	MW	3.04
	Sum, outlet exergy flow	**MW**	**766.5**
	Total irreversibility rate in the control volume	**MW**	**38.7**
	Specific irreversibility rate	**$MJ/kg_{CO2\ captured}$**	**0.391**

increasing, so is the cumulative value, which is around –2.3 kJ/mol_{CO2} as CCR approaches 100%.

5.5. Exergy balance for the separation process

Table 2 provides a summary of the exergy balance for the sub-process control volume of the CO_2 separation process. In accordance with the illustration in Fig. 7, there are three inlet exergy streams in the form of the syngas feed stream, superheated auxiliary steam for solvent regeneration, and auxiliary power. Furthermore, the control volume has three outlet exergy streams in form of two product streams following the separation, as well as saturated water following the rejection of heat when the auxiliary steam is de-superheated and condensed. The total flow of in- and outlet exergy equals 805.2 MW and 766.5 MW, respectively. This translates to a total irreversibility rate equal to 38.7 MW since the irreversibility rate of the control volume is given by the difference between the respective sums of inlet and outlet exergy flows:

$$\dot{I}_{CV} = \sum_{i=1}^{n} \dot{E}_{in,i} - \sum_{j=1}^{m} \dot{E}_{out,j} \tag{13}$$

This control volume exergy balance implies that no detailed, component-wise exergy analysis is required in order to calculate the overall irreversibility rate when the external exergy destruction associated with heat rejection from intercoolers etc. is included in the control volume. Nor is such bottom-up exergy analysis required to calculate the exergy efficiency of the overall process from Eq. (2), when all boundary crossing exergy streams are accounted for. The methods of top-down versus bottom-up exergy analysis and how they relate and can be used to validate results are exemplified and discussed in detail in Berstad et al. (2021). In the present work, the top-down approach is the predominant method since the focus is process-level exergy efficiencies.

5.6. Exergy balance for the subsequent CO_2 compression process

In addition to the CO_2 separation process, the process scheme in Fig. 7 includes a second sub-process control volume in which low-pressure CO_2 is compressed and pumped to 110 bar. Actually, this control volume includes several compressor stages, intercoolers and a pump, whereas the process is shown as a black box in the Fig. 7 process scheme. Again, as for the CO_2 capture process, only the boundary crossing exergy streams are required in order to calculate the control volume irreversibility rate from Eq. (13) and exergy efficiency from Eq. (2). The resulting exergy balance, including the irreversibility rate, is summarised in Table 3.

5.7. Exergy efficiency and the impact of efficiency criterion and ambient temperature

The exergy efficiency of post-combustion CO_2 capture processes in Section 2 is evaluated based on theoretical exergy requirements for reversible separation as benchmark. This criterion is also equal to the rational efficiency suggested by Kotas for separation processes (Kotas, 1995). Applying the Eq. (2) criterion for the MDEA-based capture process, the following efficiency figure is obtained:

$$\psi_{CO_2\ sep.} = \frac{\dot{E}_{in,\ min.\ th.}}{\dot{E}_{in,\ act.}} = \frac{-5.90\ \text{MW}}{3.31\ \text{MW} + (32.50\ \text{MW} - 3.04\ \text{MW})} = -18.0\% \tag{14}$$

Furthermore, applying the same efficiency criterion for the CO_2 compression process, gives:

$$\psi_{CO_2\ compr.} = \frac{\dot{E}_{in,\ min.\ th.}}{\dot{E}_{in,\ act.}} = \frac{19.59\ \text{MW}}{34.0\ \text{MW}} = 57.6\% \tag{15}$$

The negative sign of efficiency for the separation sub-process is caused by the negative numerator, the causes behind which are explained in Sections 5.2-5.4. In addition to the exergy efficiency of the respective sub-processes, the efficiency of the total combined process of separating and compressing CO_2 can be calculated by again applying the same criterion based on the exergy streams crossing the total control volume enclosing both sub-processes. This calculation gives the following result:

$$\psi_{CO_2\ sep.\ and\ compr.} = \frac{\dot{E}_{in,\ min.\ th.}}{\dot{E}_{in,\ act.}} = \frac{13.68\ \text{MW}}{3.31\ \text{MW} + (32.50\ \text{MW} - 3.04\ \text{MW}) + 34.0\ \text{MW}} = 20.5\% \tag{16}$$

From the numerical result in Eq. (16) it can be observed that despite the negative stand-alone efficiency of the capture sub-process, the efficiency of the overall process is still positive. When considering the full control volume including both sub-processes, the minimum exergy requirement for the combined process has, unlike the stand-alone sub-process for MDEA scrubbing, a positive sign. Consequently, the efficiency also becomes positive. Another explanation is that the overall efficiency becomes a linear combination of the respective exergy efficiencies, which are weighted by the stand-alone exergy input as a fraction of the total exergy input. This can be observed from the general expression in Eq. (12), derived for the relation between sub-process efficiencies and overall efficiency. This relation can now be checked numerically against the result from Eq. (16) as follows:

$$\psi = \frac{1}{\sum_{i=I}^{II} \dot{E}_{in,i}} \cdot \sum_{i=I}^{II} \left(\psi_i \cdot \dot{E}_{in,i}\right) = \frac{-0.180 \cdot 32.77\ \text{MW} + 0.576 \cdot 34.0\ \text{MW}}{32.77\ \text{MW} + 34.0\ \text{MW}} = 20.5\% \tag{17}$$

It is thus shown that the exergy efficiency expressions in Eqs. (2) and (12) yield the same result for the overall process, provided that the criterion of Eq. (2) is used to define the stand-alone efficiency for each sub-process.

It should be added that in the literature, several alternative definitions of exergy efficiency have been proposed (Marmolejo-Correa and Gundersen, 2012). One interesting efficiency definition applicable to the CO_2 separation and CO_2 compression sub-processes, as well as the combination of both processes, is a more general rational efficiency criterion suggested by Kotas (1995). Here, all exergy changes or exergy transfers occurring inside a control volume is defined either as a desired output or as a necessary input, such that the following condition is fulfilled:

$$\sum_{i=I}^{n} \Delta \dot{E}_{in,i} = \sum_{i=I}^{m} \Delta \dot{E}_{out,i} + \dot{I}_{CV} \tag{18}$$

Table 3
Exergy balance for the sub-process control volume of the CO_2 compression process.

Inlet exergy streams	Low-pressure CO_2 exergy flow	MW	44.3
	CO_2 compression power exergy flow	MW	34.0
	Sum, inlet exergy flow	**MW**	**78.3**
Outlet exergy streams	Compressed CO_2 exergy flow	MW	63.9
	Sum, outlet exergy flow	**MW**	**63.9**
	Total irreversibility rate in the control volume	**MW**	**14.4**
	Specific irreversibility rate	**$MJ/kg_{CO2\ captured}$**	**0.145**

The rational efficiency is defined as:

$$\psi = \frac{\sum_{i=I}^{m} \Delta \dot{E}_{out,i}}{\sum_{i=I}^{n} \Delta \dot{E}_{in,i}} \tag{19}$$

For the MDEA-based CO_2 separation process, the exergy transfers can be grouped as:

Desired output, $\Delta \dot{E}_{out}$:

- Increase in chemical exergy from feed to products: 11.27 MW

Necessary inputs, $\Delta \dot{E}_{in}$:

- Decrease/sacrifice of thermomechanical exergy: 17.17 MW
- Auxiliary power input: 3.31 MW
- Auxiliary exergy input from condensation of steam: 29.46 MW

It can be observed that the irreversibility rate calculated from the balance in Eq. (18) and the above categorisation of output and input equals 38.7 MW, and therefore equals the irreversibility rate declared in Table 2. The resulting rational efficiency based on Eq. (19) becomes 22.6% for the CO_2 capture sub-process.

The categorisation of necessary exergy input and desired output for the CO_2 compression sub-process is more straightforward and gives a rational efficiency of 57.6%, which is identical to that calculated from Eq. (2):

Desired output, $\Delta \dot{E}_{out}$:

- Increase in thermomechanical exergy: 19.59 MW

Necessary input, $\Delta \dot{E}_{in}$:

- Auxiliary power input: 34.00 MW

Finally, the exergy transfers in the overall CO_2 separation and compression process can be grouped by combining the above categorisations for the sub-processes, and placing the *net* thermomechanical exergy increase in the group of desired outputs:

Desired outputs, $\Delta \dot{E}_{out}$:

- Increase in chemical exergy: 11.27 MW
- Net increase in thermomechanical exergy: 2.42 MW

Necessary inputs, $\Delta \dot{E}_{in}$:

- Auxiliary power input: 37.31 MW
- Auxiliary exergy input from condensation of steam: 29.46 MW

This grouping of exergy transfers results in a rational efficiency of 20.5%, which is equal to that produced by the Eq. (2) criterion. A summary and comparison of efficiencies based on Eqs. (2), (19) and (12) for sub-processes and the overall process is provided in Table 4. For the CO_2 capture sub-process it is obvious that the respective exergy efficiency figures, 22.6% based on desired output vs. necessary input, and –18.0% based on minimum theoretical exergy input and actual input, give very different impressions at first glance. However, this follows the different criteria. Despite producing efficiency figures of different signs, actually they do not contradict one another. As can be further observed, they provide identical results for the CO_2 compression sub-process. Moreover, *even when expressed as a function of the negative exergy efficiency of the* CO_2 *separation sub-process* in Eq. (17), the exergy efficiency of the overall process equals the figure obtained through the rational efficiency criterion in Eq. (19) as well as that in Eq. (2). Finally, the last row in Table 4 shows how the exergy efficiency figures based on Eq. (2) change if the ambient temperature T_0 is raised from 288 K to 298 K. Since the minimum theoretical exergy requirement as well as the exergy flows for material streams in the processes change with T_0, so do the resulting exergy efficiencies. Raising T_0 by 10 K results in a 3.8 percentage point increase in overall exergy efficiency, from 20.5% to 24.3%.

The rational efficiency criterion in Eq. (19) provides efficiency numbers between 0 and 1 (0–100%) but requires a predefined grouping of exergy transfers into desired outputs and necessary inputs, that must be defined by the user. As has been made clear in Marmolejo-Correa and Gundersen (2012), several definitions of exergy efficiency leave room for interpretations to a lesser or greater extent regarding what is considered exergy input and useful output, and such makes it possible in principle to calculate different efficiency numbers for a given process.

The exergy efficiency criterion in Eq. (2), and predominantly used in this work, is rigidly defined and requires no predefined grouping of exergy transfer terms. In this respect, it can be argued that our approach provides an unprejudiced measure, which for most cases is expected to give the same result as the Eq. (19) criterion. On the other hand, in instances of negative values for $\dot{E}_{in,min.th.}$, the efficiency figure cannot be interpreted in the same way as efficiencies within the 0 and 1 interval. In theory, it can take any numerical value in the interval between $-\infty$ and $+\infty$, including a singularity for the special case of $\dot{E}_{in,act.} = 0$. As exemplified in Table 4, the two methods can still yield the same result. They will, however, differ for sub-processes that are characterised by a negative minimum theoretical exergy requirement, as exemplified in this work.

It should be mentioned that negative values for minimum theoretical exergy requirement and thus negative exergy efficiency have been identified and discussed in other works, such as Nguyen et al. (2014) and Voldsund et al. (2014), with respect to offshore oil and gas processing platforms. For one facility, the reductions in thermomechanical exergy was found to be substantially higher than the increases in chemical exergy, that is, qualitatively the same observation made for the MDEA-based CO_2 capture process in the present work. Furthermore, the negative efficiency figure was considered to illustrate a limitation of the applicability of this particular exergy efficiency definition and instead, a different component-by-component criterion was applied (Nguyen et al., 2014).

However, based on the examples provided in this work, the criterion which in one instance results in negative efficiency on a sub-process level is still applicable in principle as it can be used as input to calculate the overall process efficiency through the linear combination of sub-process exergy efficiencies in Eq. (12). Moreover, as shown in Table 4, it does not contradict the alternative rational efficiency criterion with respect to overall process efficiency.

Table 4
Comparison of exergy efficiency results for sub-processes and the overall process.

Exergy efficiency criterion	CO_2 separation	CO_2 compression	Overall process
Eq. (2) Exergy efficiency	–18.0%	57.6%	20.5%
Eq. (19) Rational efficiency	22.6%	57.6%	20.5%
Eq. (12) Combined sub-process efficiencies	–18.0%	57.6%	20.5%
Eq. (2) Exergy efficiency (T_0 = 298 K)	–20.5%	62.0%	24.3%

6. Conclusions

The most common targets for minimum theoretical separation work for CO_2 capture found in the literature are based on the assumptions of ideal gas conditions and isothermal separation, as well as equal pressure for the feed and product streams. Comparison of this methodology and assumptions with results from rigorous simulations based on the Peng–Robinson equation of state, suggests that ideal gas-based approximations are useful for conditions where the pressure and temperature level of flue gas and separation products are close to ambient conditions. Through numerical examples it has been shown that ideal gas assumptions become less accurate for quantifying exergy targets for a range of other relevant separation process conditions, even when the assumptions of isobaric and isothermal separation are still used. With increasing pressure level, the ideal gas assumption becomes increasingly inaccurate.

Whereas the changes in chemical exergy in the context of gas separation can be estimated with the ideal gas assumption provided that the mixtures are close to ideal at ambient conditions, calculating the changes in thermomechanical exergy may require more adequate thermophysical property models. This is required for several common separation processes that include considerable changes in temperature and pressure, for instance solvent processes for syngas absorbing CO_2 at high pressure and discharging at low pressure. To reveal minimum targets for exergy requirement for any given separation process, regardless of feed and product conditions, a more general exergy targeting method has therefore been implemented in process simulation software.

A general expression has been derived for the relation between stand-alone exergy efficiencies for sub-processes in a larger system, and that of the overall system made up of the different sub-processes. It has been shown that it is possible to express the overall exergy efficiency as a linear combination of stand-alone sub-process efficiencies, where the weighting factors are the fractions of the exergy input to each sub-process relative to the exergy input to the overall process.

It has been shown that sub-processes for CO_2 separation may actually have a negative value for minimum separation work, implying that a reversible separation process subject to the defined boundary conditions would deliver the defined product streams at respective specified thermodynamic states and simultaneously yield a net exergy output. At the same time, it has been shown that real processes, in this case an MDEA solvent process for CO_2 capture from high-pressure syngas, may well require a substantial exergy input despite having such a negative value for minimum theoretical separation work. Based on the defintion used throughout this work, the exergy efficiency thus becomes negative. Even with a negative sub-process efficiency for the CO_2 separation unit, consistency is still observed in the form of identical results when calculating the overall system efficiency in one of the following two ways: (1) finding the ratio between minimum exergy requirement and actual exergy input for the overall process, and (2) finding the same ratio for the individual sub-processes and then combining them linearly by using weighting factors.

Exergy efficiencies obtained from the efficiency definition used throughout this work have been compared with corresponding results obtained by the well-established rational exergy efficiency. It has been found that there is no conflict or contradiction between the two efficiency criteria as long as they are applied consistently. They rather represent two partly different means for defining and assessing exergy efficiency. As exemplified by the numerical results, they will in many instances produce equal results, which is the case for the CO_2 compression sub-process as well as for the combined CO_2 separation and compression process. The main difference between the definitions is revealed in cases where a negative sign for the minimum theoretical exergy requirement is encountered. When this coincides with an actual exergy requirement with a positive sign, the first efficiency definition yields a negative figure for exergy efficiency. In other words, when a process that would provide a net exergy output in reversible mode instead requires a net exergy input in the real case, this is interpreted as giving a negative exergy efficiency.

Declaration of Competing Interest

The authors declare that they have no known competing financial interests or personal relationships that could have appeared to influence the work reported in this paper.

Acknowledgments

The authors acknowledge the Research Council of Norway for basic funding supporting this work.

References

Amrollahi, Z., Ertesvåg, I.S., Bolland, O., 2011a. Thermodynamic analysis on post-combustion CO_2 capture of natural-gas-fired power plant. Int. J. Greenh. Gas Control 5, 422–426. doi:10.1016/j.ijggc.2010.09.004.

Amrollahi, Z., Ertesvåg, I.S., Bolland, O., 2011b. Optimized process configurations of post-combustion CO_2 capture for natural-gas-fired power plant—exergy analysis. Int. J. Greenh. Gas Control 5, 1393–1405. doi:10.1016/j.ijggc.2011.09.004.

Berstad, D., Anantharaman, R., Nekså, P., 2013. Low-temperature CO_2 capture technologies—applications and potential. Int. J. Refrig. 36, 1403–1416.

Berstad, D., Skaugen, G., Wilhelmsen, Ø., 2021. Dissecting the exergy balance of a hydrogen liquefier: analysis of a scaled-up Claude hydrogen liquefier with mixed refrigerant pre-cooling. Int. J. Hydrogen Energy 46, 8014–8029.

Cao, Y., He, B., Ding, G., Su, L., Duan, Z., 2017. Energy and exergy investigation on two improved IGCC power plants with different CO_2 capture schemes. Energy 140, 47–57. doi:10.1016/j.energy.2017.08.044.

Edwards, C.F., Brandt, A.R., Calbry-Muzyka, A., Sun, Y., 2015. Carbon Capture Systems Analysis: Comparing Exergy Efficiency and Cost of Electricity of Existing and Future Technology Options. Progress Report. https://gcep.stanford.edu/pdfs/techreport2015/2.3.5%20Edwards%20(s&p).pdf (accessed 10 January 2023).

Erans, M., Sanz-Pérez, E.S., Hanak, D.P., Clulow, Z., Reiner, D.M., Mutch, G.A., 2022. Direct air capture: process technology, techno-economic and socio-political challenges. Energy Environ. Sci. 15, 1360–1405.

Ertesvåg, I.S., Kvamsdal, H.M., Bolland, O., 2005. Exergy analysis of a gas-turbine combined-cycle power plant with precombustion CO_2 capture. Energy 30, 5–39. doi:10.1016/j.energy.2004.05.029.

Feyzi, V., Beheshti, M., Kharaji, A.G., 2017. Exergy analysis: a CO_2 removal plant using a-MDEA as the solvent. Energy 118, 77–84. doi:10.1016/j.energy.2016.12.020.

Geuzebroek, F.H., Schneiders, L.H.J.M., Kraaijveld, G.J.C., Feron, P.H.M., 2004. Exergy analysis of alkanolamine-based CO_2 removal unit with AspenPlus. Energy 29, 1241–1248. doi:10.1016/j.energy.2004.03.083.

Herzog H., Meldon J., Hatton A. (2009). Advanced Post-Combustion CO2 Capture. https://sequestration.mit.edu/pdf/Advanced_Post_Combustion_CO2_Capture.pdf

Jordal, K., Anantharaman, R., Peters, T.A., Berstad, D., Morud, J., Nekså, P., Bredesen, R., 2015. High-purity H_2 production with CO_2 capture based on coal gasification. Energy 88, 9–17. doi:10.1016/j.energy.2015.03.129.

Kotas, T.J., 1995. The Exergy Method of Thermal Plant Analysis. Krieger Publishing Company, Melbourne, FL, USA reprinted. https://doi.org/10.1016/C2013-0-00894-8.

Marmolejo-Correa, D., Gundersen, T., 2012. A comparison of exergy efficiency definitions with focus on low temperature processes. Energy 44, 477–489.

Moioli, S., Giuffrida, A., Romano, M.C., Pellegrini, L.A., Lozza, G., 2016. Assessment of MDEA absorption process for sequential H_2S removal and CO_2 capture in air-blown IGCC plants. Appl. Energy 183, 1452–1470.

Moioli, S., Pellegrini, L.A., Romano, M.C., Giuffrida, A., 2017. Pre-combustion CO_2 removal in IGCC plant by MDEA scrubbing: modifications to the process flowsheet for energy saving. Energy Procedia 114, 2136–2145.

Nguyen, T.V., Voldsund, M., Elmegaard, B., Ertesvåg, I.S., Kjelstrup, S., 2014. On the definition of exergy efficiencies for petroleum systems: application to offshore oil and gas processing. Energy 73, 264–281. doi:10.1016/j.energy.2014.06.020.

Nord, L., Bolland, O., 2020. Carbon Dioxide Emission Management in Power Generation. Wiley-VCH, Weinheim.

Oh, H.T., Kum, J., Park, J., Vo, N.D., Jun-Ho Kang, J.H., Lee, C.H, 2022. Pre-combustion CO_2 capture using amine-based absorption process for blue H_2 production from steam methane reformer. Energy Convers. Manag. 262, 115632. doi:10.1016/j.enconman.2022.115632.

Rochedo, P.R.R., Szklo, A., 2013. Designing learning curves for carbon capture based on chemical absorption according to the minimum work of separation. Appl. Energy 108, 383–391. doi:10.1016/j.apenergy.2013.03.007.

Rochelle, G., Chen, E., Freeman, S., Van Wagener, D., Xu, Q., Voice, A., 2011. Aqueous piperazine as the new standard for CO_2 capture technology. Chem. Eng. J. 171, 725–733.

Sato, N., 2004. Chemical Energy and Exergy. An Introduction to Chemical Thermodynamics For Engineers. Elsevier, Amsterdam, The Netherlands.

Voldsund, M., Nguyen, T.-.V., Elmegaard, B., Ertesvåg, I.S., Røsjorde, A., Jøssang, K., Kjelstrup, S., 2014a. Exergy destruction and losses on four North Sea offshore platforms: a comparative study of the oil and gas processing plants. Energy 74, 45–58. doi:10.1016/j.energy.2014.02.080.

Voldsund, M., Nguyen, T.V., Elmegaard, B., Ertesvåg, I.S., Kjelstrup, S., 2014b. Thermodynamic performance indicators for offshore oil and gas processing: application to four North Sea facilities. Oil Gas Fac. 3, 051–063.

Wilcox, J., 2012. Carbon Capture. Springer-Verlag, New York.

Zhao, R., Deng, S., Liu, Y., Zhao, Q., He, J., Zhao, L., 2017. Carbon pump: fundamental theory and applications. Energy 119, 1131–1143.